Supplemental Material: Spatiotemporal control of structure in a polar active fluid

Saptorshi Ghosh[1], Chaitanya Joshi[2], Aparna Baskaran[1*] and Michael F. Hagan[1†]
[1]*Physics Department, Brandeis University, Waltham, Massachusetts 02453, USA*
[2]*Department of Physics and Astronomy, Tufts University, Medford, Massachusetts 02155, USA*

I. MOMENT OF INERTIA

The moment of inertia matrix for the aster is given by

$$\mathcal{I}_{ij} = \sum_k m_k \left(||r_k||^2 \delta_{ij} - x_i^k x_j^k \right) \tag{1}$$

with m_k a mask to restrict the calculation to the vicinity of the aster:

$$m_k = \Theta(\rho(x,y) - \rho_0) \tag{2}$$

where Θ is the Heaviside step function and ρ is the density field. That is, m_k is the density field value at all points with density above the mean value; otherwise $m_k = 0$. The aster's center of mass is dynamically tracked, and x_i^k represents the distance of the k-th point from the i-th axis, which passes through aster's center of mass.

Upon diagonalizing this moment of inertia matrix, we obtain the eigenvalues λ_1 and λ_2, which correspond to the principal moments of inertia. We then define the *asphericity* as the ratio $\frac{\lambda_2}{\lambda_1}$, which quantifies the extent of non-sphericity (asphericity) of the moving object.

A ratio closer to 1 indicates a more spherical shape, while significantly deviating values suggest an elongated or flattened form.

II. ORIENTATION FIELD

We further quantify the motion of aster by measuring the orientation of polarization vectors relative to the polar axis. The reference point of the polar axis is determined by the point where density field has the maximum value. Our region of interest is a circular region of radius ~ 10 (in non-dimensional units), which is roughly the radius of an aster. We mask out the remaining space. This is depicted in the inset to Figure 2 in the main text, where the circle approximates the aster.

III. ANALYZING THE OPTIMAL CONTROL SOLUTION: CALCULATING THE TORQUE

We start with the full hydrodynamic equation for polarization:

$$\begin{aligned} \partial_t \boldsymbol{\tau} = -(a_2(\rho) + a_4(\rho)|\boldsymbol{\tau}|^2)\boldsymbol{\tau} - \boldsymbol{\nabla}(\omega\rho) + \boldsymbol{\nabla}^2\boldsymbol{\tau} + \\ \lambda \left(\boldsymbol{\tau}_\alpha \boldsymbol{\nabla} \boldsymbol{\tau}_\alpha + \boldsymbol{\tau}\boldsymbol{\nabla}.\boldsymbol{\tau} - \boldsymbol{\tau}.\boldsymbol{\nabla}\boldsymbol{\tau} \right). \end{aligned} \tag{3}$$

During the initial stages, the applied activity profile exhibits large spatial gradients, with the predominant contribution to polarization dynamics largely stemming from the term $\nabla(\omega\rho)$:

$$\partial_t \boldsymbol{\tau} = -\rho \boldsymbol{\nabla} \omega \tag{4}$$

We express $\boldsymbol{\tau} = |\boldsymbol{\tau}|[cos\theta\hat{x} + sin\theta\hat{y}]$, and re-write equation (4) as:

$$|\boldsymbol{\tau}| \partial_t \left[\cos\theta \hat{\boldsymbol{x}} + \sin\theta \hat{\boldsymbol{y}} \right] = -\rho \left[\partial_x \omega \hat{\boldsymbol{x}} + \partial_y \omega \hat{\boldsymbol{y}} \right] \tag{5}$$

* aparna@brandeis.edu
† hagan@brandeis.edu

Further simplification yields:

$$|\boldsymbol{\tau}|\partial_t\theta\left[-\sin\theta\hat{\boldsymbol{x}}+\cos\theta\hat{\boldsymbol{y}}\right]=-\rho\left[\partial_x\omega\hat{\boldsymbol{x}}+\partial_y\omega\hat{\boldsymbol{y}}\right] \tag{6}$$

$$|\boldsymbol{\tau}|\partial_t\theta=\rho\left[\partial_x\omega\sin\theta-\partial_y\omega\cos\theta\right]. \tag{7}$$

Finally, this formulation results in:

$$\partial_t\theta\sim\boldsymbol{\nabla}\omega\times\hat{\boldsymbol{\tau}}/|\boldsymbol{\tau}|, \tag{8}$$

where the expression (8) elucidates the temporal evolution of θ influenced by the cross product of the gradient of activity $\boldsymbol{\nabla}\omega$ and the unit vector $\hat{\boldsymbol{\tau}}$ in the direction of the torque $\boldsymbol{\tau}$, normalized by the magnitude of $\boldsymbol{\tau}$.

IV. DIRECT-ADJOINT-LOOPING (DAL) METHOD

We use direct-adjoint-looping (DAL), an iterative optimization method [1] to solve for optimal schedule of activity in space and time that accomplishes our control goals. We start by writing the Lagrangian $\mathcal{L}$ of optimization, Eq. (**??**), where $\boldsymbol{\nu}$ and η act as Lagrange multipliers or adjoint variables that constrain the dynamics to follow Eqs. (**??**) and (3).

We construct an initial condition by performing a simulation with unperturbed dynamics (Eqs. (**??**) and (3)) until reaching steady-state, at a parameter set that leads to a desired initial behavior. We construct a target configuration in the same manner, using a different parameter set that leads to the desired target behavior. We also specify a time duration t_{F} over which the control protocol will be employed, and an initial trial control protocol $\omega^0(\mathbf{r},t)$. We then perform a series of DAL iterations, with each iteration involving the following steps:

- **Step 1:** The equations of motion, (**??**) and (3), are integrated forward in time from $t=0$ to $t=t_{\mathrm{F}}$ with the current protocol of spatiotemporal activity $\omega^i(\mathbf{r},t)$ (where i is the current iteration) and fixed initial conditions, $\rho(\mathbf{r},0)$ and $\tau(\mathbf{r},0)$.
- **Step 2:** The adjoint equations, (**??**) and (**??**), are integrated backward in time from $t=t_{\mathrm{F}}$ to $t=0$ with the initial condition, $\eta(\mathbf{r},t_{\mathrm{F}})=0$ and $\boldsymbol{\nu}(\mathbf{r},t_{\mathrm{F}})=0$.
- **Step 3:** The control protocol is updated via gradient descent, $\omega^{i+1}=\omega^i-\Delta\delta\mathcal{J}/\delta\omega$, to minimize the cost function.

Iterations are continued until the gradient $\delta\mathcal{J}/\delta\omega$ falls below a user-defined tolerance. We employ Armijo backtracking [2] to adaptively choose the step-size Δ for gradient descent and to ensure convergence of the DAL algorithm.

V. DERIVATION OF ADJOINT EQUATIONS

We begin with the equation of motion for the state variables:

$$\partial_t\rho=-\boldsymbol{\nabla}\cdot(\bar{\omega}^2\boldsymbol{\tau}-\boldsymbol{\nabla}\rho) \tag{9}$$

$$\begin{aligned}\partial_t\boldsymbol{\tau}=-(a_2(\rho)+a_4(\rho)|\boldsymbol{\tau}|^2)\boldsymbol{\tau}-\boldsymbol{\nabla}(\bar{\omega}^2\rho)+\boldsymbol{\nabla}^2\boldsymbol{\tau}+\\ \lambda\left(\boldsymbol{\tau}_\alpha\boldsymbol{\nabla}\boldsymbol{\tau}_\alpha+\boldsymbol{\tau}\boldsymbol{\nabla}.\boldsymbol{\tau}-\boldsymbol{\tau}.\boldsymbol{\nabla}\boldsymbol{\tau}\right).\end{aligned} \tag{10}$$

We write the full objective function, which is the sum of terminal state and running state penalties that we aim to minimize, as follows:

$$\mathcal{J}=\frac{1}{2}\int_\Omega d\mathbf{r}\,E\left(\rho_{t_{\mathrm{F}}}-\rho^*\right)^2+F\left(\boldsymbol{\tau}_{t_{\mathrm{F}}}-\boldsymbol{\tau}^*\right)^2+\int_o^{t_{\mathrm{F}}}dt\int_\Omega d\mathbf{r}\mathcal{H},$$

where,

$$\mathcal{H}=\left[\frac{A}{2}\left(\bar{\omega}^2-\omega_0^2\right)^2+\frac{B}{2}\boldsymbol{\nabla}\bar{\omega}^2\cdot\boldsymbol{\nabla}\bar{\omega}^2+\frac{K}{2}(d\bar{\omega}^2/dt)^2+\frac{C}{2}\left(\rho-\rho^*\right)^2+\frac{D}{2}\left(\boldsymbol{\tau}-\boldsymbol{\tau}^*\right)^2\right]. \tag{11}$$

We then introduce Lagrange multipliers η and $\boldsymbol{\nu}$ that constrain the dynamics to the equations of motion for density and polarization respectively, and write the Lagrangian as:

$$\mathcal{L} = \mathcal{J} + \int_0^{t_{\rm F}} dt \int_\Omega d\mathbf{r}\eta \left[\partial_t \rho + \boldsymbol{\nabla}\cdot(\bar{\omega}^2\boldsymbol{\tau} - \boldsymbol{\nabla}\rho)\right] + \boldsymbol{\nu}\cdot\left[\partial_t\boldsymbol{\tau} + (a_2 + a_4|\boldsymbol{\tau}|^2)\boldsymbol{\tau} + \boldsymbol{\nabla}(\bar{\omega}^2\rho) - \boldsymbol{\nabla}^2\boldsymbol{\tau} - \lambda\left(\tau_\alpha\boldsymbol{\nabla}\tau_\alpha + \boldsymbol{\tau}\boldsymbol{\nabla}\cdot\boldsymbol{\tau} - \boldsymbol{\tau}\cdot\boldsymbol{\nabla}\boldsymbol{\tau}\right)\right]. \tag{12}$$

The necessary condition for optimality is $\nabla\mathcal{L} = 0$ [3, 4], so $\delta\mathcal{L}/\delta\eta$, $\delta\mathcal{L}/\delta\boldsymbol{\nu}$, $\delta\mathcal{L}/\delta\rho$, $\delta\mathcal{L}/\delta\boldsymbol{\tau}$, $\delta\mathcal{L}/\delta\rho(t_{\rm F})$, $\delta\mathcal{L}/\delta\boldsymbol{\tau}(t_{\rm F})$, and $\delta\mathcal{L}/\delta\bar{\omega} = 0$. The first two conditions of optimality yield back the dynamics equations. The next two conditions, $\delta\mathcal{L}/\delta\rho$, $\delta\mathcal{L}/\delta\boldsymbol{\tau}$, yield dynamics equations for the adjoint variables η and $\boldsymbol{\nu}$ as:

$$\begin{aligned}\partial_t\eta =& C(\rho - \rho^*) - \boldsymbol{\nabla}^2\eta - \bar{\omega}^2\boldsymbol{\nabla}\cdot\boldsymbol{\nu} \\ &+ (\delta_\rho a_2(\rho) + \delta_\rho a_4(\rho)|\boldsymbol{\tau}|^2)(\boldsymbol{\nu}.\boldsymbol{\tau}).\end{aligned} \tag{13}$$

$$\begin{aligned}\partial_t\boldsymbol{\nu} =& D(\boldsymbol{\tau} - \boldsymbol{\tau}^*) + \left(a_2(\rho) + a_4(\rho)|\boldsymbol{\tau}|^2\right)\boldsymbol{\nu} + 2a_4(\rho)\boldsymbol{\tau}(\boldsymbol{\nu}\cdot\boldsymbol{\tau}) \\ &- \lambda\left[-\boldsymbol{\tau}\boldsymbol{\nabla}\cdot\boldsymbol{\nu} + 2\boldsymbol{\nu}\boldsymbol{\nabla}\cdot\boldsymbol{\tau} - \boldsymbol{\nabla}(\boldsymbol{\nu}\cdot\boldsymbol{\tau})\right. \\ &\left.+\boldsymbol{\tau}\cdot\boldsymbol{\nabla}\boldsymbol{\nu} - \boldsymbol{\nu}_{\boldsymbol{\alpha}}\boldsymbol{\nabla}\boldsymbol{\tau}_{\boldsymbol{\alpha}}\right] - \boldsymbol{\nabla}^2\boldsymbol{\nu} - \bar{\omega}^2\boldsymbol{\nabla}\eta.\end{aligned} \tag{14}$$

with a boundary condition at time $t_{\rm F}$ set by $\delta\mathcal{L}/\delta\rho(t_{\rm F})$, $\delta\mathcal{L}/\delta\boldsymbol{\tau}(t_{\rm F})$ as $\eta(t_{\rm F}) = -E(\rho(t_{\rm F}) - \rho^*) = 0$ and $\boldsymbol{\nu}(t_{\rm F}) = -F(\boldsymbol{\tau}(t_{\rm F}) - \boldsymbol{\tau}^*)$. For our computations, we choose $E, F = 0$ for simplicity since we obtained adequate convergence from the time-integrated penalty.

Finally, the condition $\delta\mathcal{L}/\delta\bar{\omega}$ yields:

$$\delta\mathcal{L}/\delta\bar{\omega} = 2A\bar{\omega}\left(\bar{\omega}^2 - \omega_0^2\right) - 2B\bar{\omega}\boldsymbol{\nabla}^2\bar{\omega}^2 - 2K\bar{\omega}(d^2\bar{\omega}^2/dt^2) - 2\bar{\omega}\boldsymbol{\tau}\cdot\boldsymbol{\nabla}\eta - 2\bar{\omega}\boldsymbol{\nu}\cdot\boldsymbol{\nabla}\rho. \tag{15}$$

which is used to update the control variable $\bar{\omega}$ ($\sqrt{\omega}$) during gradient descent.

VI. CONTROLLABILITY

Let us consider the problem we want to solve in control theory. If we define $\mathbf{X} = \begin{pmatrix}\rho \\ \tau_{\rm x} \\ \tau_{\rm y}\end{pmatrix}$, we seek to solve the set of nonlinear partial differential equations $\frac{\partial\mathbf{X}}{\partial t} = H[\mathbf{X}, \omega]$ for the control solution $\omega(\mathbf{r}, t)$, subject to a given initial condition $X(\mathbf{r}, 0)$, and a boundary condition in time $X(\mathbf{r}, t_{\rm F})$, which is the target state with $\{0, t_{\rm F}\}$ as the control window. A particular dynamical system is considered controllable if we can demonstrate the existence of a solution to the above problem. When the dynamics is nonlinear, demonstrations of controllability have been limited to a few simple systems where the nonlinearities have special properties. What we do instead is consider the controllability of Eqs. **??** -3 when linearized about the unstable fixed point of a homogeneous polar state. Demonstrating controllability of the homogeneous fixed point tells us that at short enough length scales, we will be able to drive the system to desired values of the dynamical fields, which can be thought of as different fixed points in the continuous space of fixed points associated with translational symmetry and broken rotational symmetry characteristic of our system.

Linearizing our theory using $\rho = \rho_0 + \delta\rho(\boldsymbol{r}, t)$ and $\boldsymbol{\tau} = \boldsymbol{\tau_0} + \delta\tau_\parallel(\boldsymbol{r}, t)\hat{x} + \delta\tau_\perp(r, t)\hat{y}$, and introducing the Fourier transform, $\tilde{x}(\boldsymbol{q}, t) = \int d\boldsymbol{r}e^{i\boldsymbol{q}\cdot\boldsymbol{r}}x(\boldsymbol{r}, t)$, we obtain

$$\partial_t\begin{pmatrix}\delta\tilde{\rho} \\ \delta\tilde{\tau}_\parallel \\ \delta\tilde{\tau}_\perp\end{pmatrix} = \begin{pmatrix}-q^2 & i\omega q_\parallel & i\omega q_\perp \\ \alpha_1(\rho_0) + i\omega q_\parallel & -\left(\alpha_2 + i\lambda\tau_0 q_\parallel + q^2\right) & -i\lambda\tau_0 q_\perp \\ i\omega q_\perp & -i\lambda\tau_0 q_\perp & i\lambda\tau_0 q_\parallel - q^2\end{pmatrix}\begin{pmatrix}\delta\tilde{\rho} \\ \delta\tilde{\tau}_\parallel \\ \delta\tilde{\tau}_\perp\end{pmatrix} + \begin{pmatrix}i\tau_0 q_\parallel \\ i\rho_0 q_\parallel \\ i\rho_0 q_\perp\end{pmatrix}\delta\tilde{\omega}$$

where $q_{\parallel,\perp}$ denote the wavevectors along and orthogonal to direction of polarization, $\alpha_1(\rho) = -\tau_0\left(\frac{\delta a_2}{\delta\rho} - \frac{a_2}{a_4}\frac{\delta a_4}{\delta\rho}\right)$, and $\alpha_2(\rho) = -2a_2$. Note that $\alpha_{1,2} > 0$ for all $\rho_0 > \rho_c$.

Let us now introduce the notation

$$X_{\rm q} = \begin{pmatrix}\delta\tilde{\rho} \\ \delta\tilde{\tau}_\parallel \\ \delta\tilde{\tau}_\perp\end{pmatrix},$$

$\omega_{\rm q} = \delta\tilde{\omega}(\mathbf{q},t)$, and

$$B_{\rm q} = \begin{pmatrix} i\tau_0 q_\parallel \\ i\rho_0 q_\parallel \\ i\rho_0 q_\perp \end{pmatrix}.$$

Our linearized theory is then of the form,

$$\partial_t X_{\rm q}(t) = A_{\rm q} X_{\rm q}(t) + B_{\rm q}\omega_{\rm q}(t)$$

One can readily establish that this linear system has a solution to the boundary value control problem when the controllability matrix

$$C = \begin{bmatrix} B_{\rm q} & A_{\rm q}B_{\rm q} & A_{\rm q}^2 B_{\rm q} \end{bmatrix}$$

is of rank 3 [5–7].

Computing the column vectors of C, we obtain

$$A_{\rm q}B_{\rm q} = \begin{bmatrix} -\omega\rho_0 q^2 - i\tau_0 q_\parallel q^2 \\ i\tau_0 q_\parallel\left(\alpha_1(\rho_0) + i\omega q_\parallel\right) - i\rho_0 q_\parallel\left(\alpha_2(\rho_0) + q^2\right) + \lambda\rho_0\tau_0 q^2 \\ -i\rho_0 q_\perp q^2 - \tau_0\omega q_\parallel q_\perp \end{bmatrix}$$

$$A^2 B = \begin{bmatrix} i\rho_0 q_\parallel\left(\lambda\tau_0\omega q^2 - i\omega q_\parallel\left(\alpha_2 + 2q^2\right)\right) \\ +i\tau_0 q_\parallel\left(i\omega q_\parallel\alpha_1 - \omega^2 q^2 - q^2\right) \\ +2\omega\rho_0 q_\perp^2 q^2 \\ \\ i\rho_0 q_\parallel\left(\left(\alpha_2 + i\lambda\tau_0 q_\parallel + q^2\right)^2 - \lambda^2\tau_0^2 q_\perp^2\right) \\ +i\rho_0 q_\perp\left(i\lambda\tau_0 q_\perp\left(\alpha_2 + 2q^2\right)\right) - \omega\rho_0 q^2\left(\alpha_1 + i\omega q_\parallel\right) \\ -i\tau_0 q_\parallel\left(\left(\alpha_1 + i\omega q_\parallel\right)\left(\alpha_2 + i\lambda\tau_0 q_\parallel - 2q^2\right) - \lambda\tau_0\omega q_\perp^2\right) \\ \\ i\rho_0 q_\parallel\left(i\lambda\tau_0 q_\perp\left(\alpha_2 + 2q^2\right) - \omega^2 q_\parallel q_\perp\right) \\ +i\tau_0 q_\parallel\left(-i\lambda\tau_0 q_\perp\alpha_1 - 2i\omega q_\perp q^2\right) \\ +i\rho_0 q_\perp\left(-\lambda^2\tau_0^2 q^2 + q^2\left(q^2 - 2i\lambda\tau_0 q_\parallel\right) - \omega^2 q_\perp^2\right) \end{bmatrix}$$

To examine the rank of the matrix C in a physically informative way, let us consider 3 special cases. First, let us consider the case of spatial gradients orthogonal to the direction of order. Setting $q_\parallel = 0$ and truncating the matrix elements to quadratic order in q we obtain

$$C = \begin{pmatrix} 0 & -\omega\rho_0 q_\perp^2 & 0 \\ 0 & \lambda\rho_0\tau_0 q_\perp^2 & -\rho_0\lambda\tau_0\alpha_2 q_\perp^2 - \omega\rho_0\alpha_1 q_\perp^2 \\ & & -\lambda\tau_0\omega q_\perp^2 \\ i\rho_0 q_\perp & 0 & 0 \end{pmatrix}$$

As is apparent from the form of the matrix, the three column vectors are indeed linearly independent and hence the linearized theory of an active polar fluid is controllable in the presence of gradients in the direction perpendicular to that of the spontaneously broken symmetry. Next, let us consider two cases that show the limits on the controllability of the linear theory. If we consider the long wavelength limit of the controllability matrix C, we see that, when truncated to lowest order in wavevector

$$C = \begin{pmatrix} i\tau_0 q_\parallel & 0 & 0 \\ i\rho_0 q_\parallel & i\tau_0 q_\parallel\alpha_1 + i\rho_0 q_\parallel\alpha_2 & i\rho_0 q_\parallel\alpha_2^2 - i\tau_0 q_\parallel\alpha_1\alpha_2 \\ i\rho_0 q_\perp & 0 & 0 \end{pmatrix}$$

which clearly is not of rank 3. Thus, the system is not controllable on the longest length scales. To identify the length scale up to which the system is controllable, let us compare the relevant terms in the second column. We will need to retain terms to quadratic order in the gradients when $\lambda\rho_0\tau_0 q_\perp^2 \sim (\rho_0\alpha_2 + \tau_0\alpha_1)q_\parallel$. Setting aside the direction of spatial homegeneity we get an estimate of the length scale up to which the system is controllable as $\ell_{\rm max} = \frac{\lambda\rho_0\tau_0}{(\rho_0\alpha_2 + \tau_0\alpha_1)}$. Given that all the terms on the right hand side scale with the mean density ρ_0, the length scale

up to which the linear system is controllable is set by the strength of the nonlinearities λ. Recall that our system is non-dimensionalized using the diffusive length scale $(D/\nu)^{1/2}$ and λ has the units of a diffusion coefficient. So, our system is controllable on length scales that are comparable to the diffusive length scale.

Finally, note that when we restrict attention to spatial gradients that lie purely along the direction of broken symmetry, the controllability matrix becomes

$$C = \begin{pmatrix} i\tau_0 q_\parallel & -i\omega_0 q_\parallel^2 & \rho_0\omega_0\alpha_2 q_\parallel^2 - \tau_0\omega_0\alpha_1 q_\parallel^2 \\ i\rho_0 q_\parallel & i\tau_0 q_\parallel \alpha_1 - i\rho_0 q_\parallel \alpha_2 & i\rho_0 q_\parallel \alpha_2^2 - i\tau_0 q_\parallel \alpha_1\alpha_2 \\ & -\tau_0\omega q_\parallel^2 + \lambda\rho_0\tau_0 q_\parallel^2 & -\omega\rho_0 q_\parallel^2\alpha_1 + \alpha_1\lambda\tau_0^2 q_\parallel^2 \\ 0 & 0 & -i\alpha_2\tau_0\omega q_\parallel^2 \\ & & 0 \end{pmatrix}$$

and the system is clearly not controllable. Thus, we see that spatial gradients orthogonal to the direction of the local polar order are critical to obtaining control solutions for an active polar fluid.

VII. RESIDUES: DEVIATIONS FROM TARGET STATE AS A FUNCTION OF TIME

In this section, we assess how quickly the solutions approach their target by plotting the residues, meaning the deviations from the target state, $(\rho - \rho^*)^2 + (\boldsymbol{\tau} - \boldsymbol{\tau}^*)^2$, and the deviation of the control variable from its baseline value, $\omega - \omega_0$. SI Figs. 1 – 4 show these residues as a function of time for the examples of: aster advection (Fig. 2 main text), aster advection with the trajectory specified (Figs.3a, 3b main text), and remodelling a stripe into an aster (Fig. 5 main text).

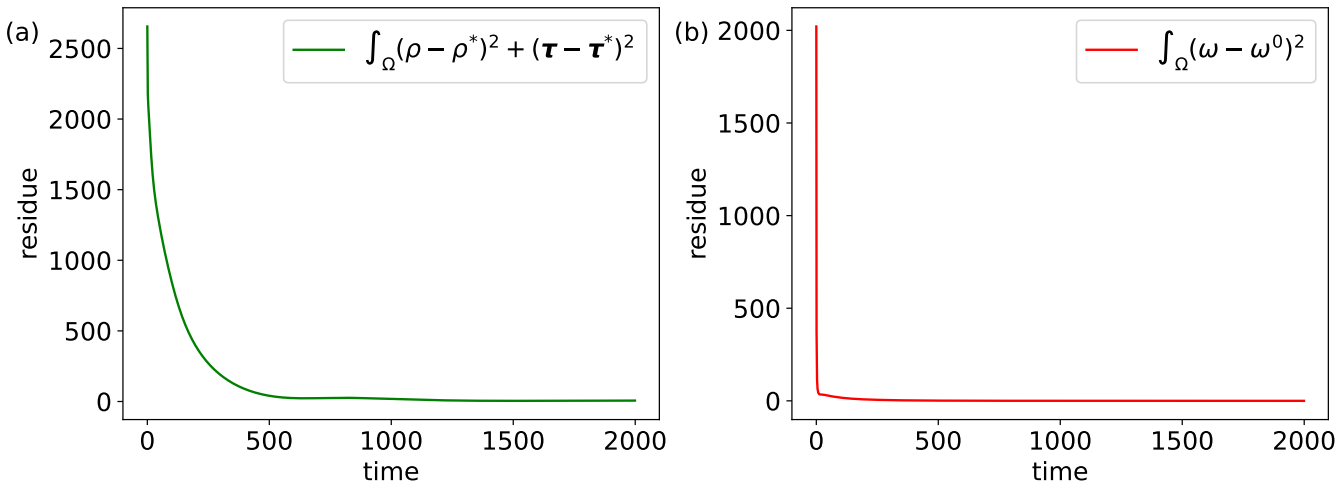

FIG. 1. **Residues as a function of time for aster advection with only initial and target state specified (Fig. 2 main text).** (a) State residue: deviation of the system state from the target. (b) Control residue: the deviation of the control variable from its baseline value.

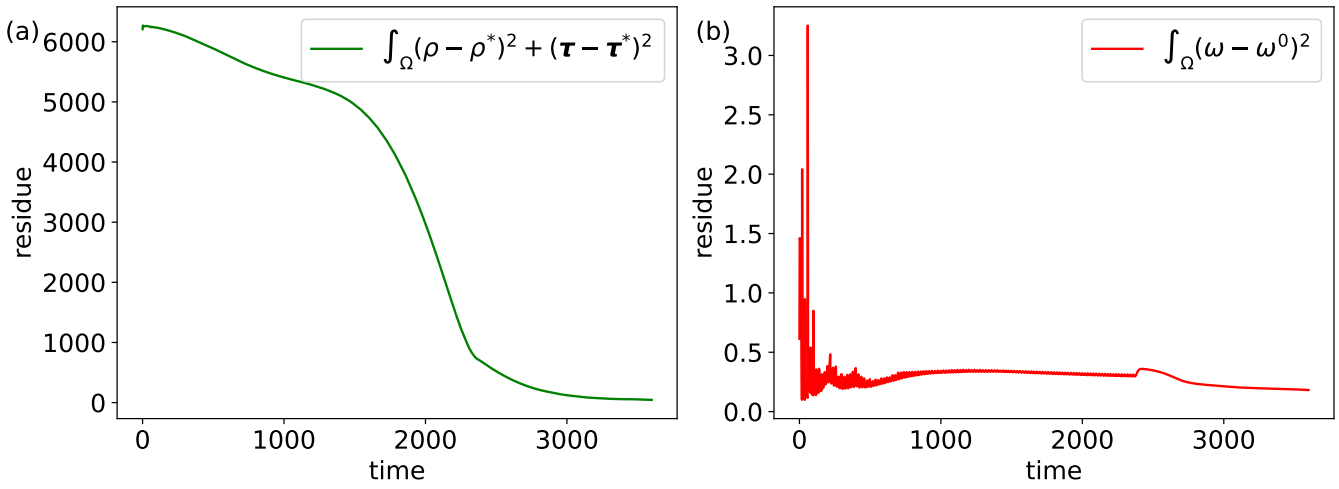

FIG. 2. **Residues for aster advection with path specified, slow advection (Aster-like trajectory, Fig. 3a main text).** (a) State residue: deviation of the system state from the target. (b) Control residue: the deviation of the control variable from its baseline value.

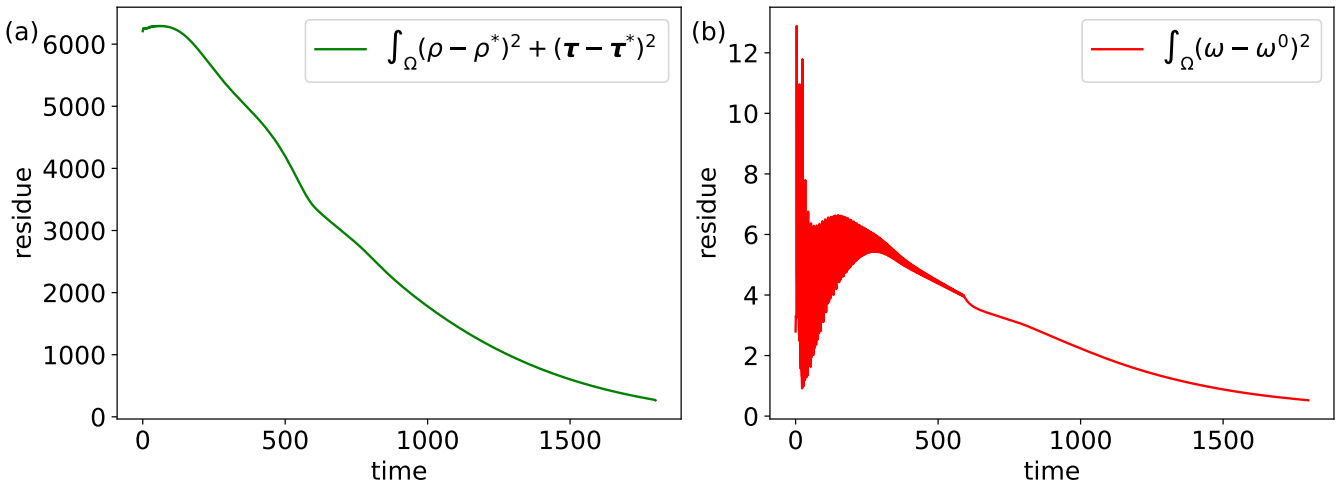

FIG. 3. **Residues for aster advection with path specified, fast advection (Flock-like trajectory, Fig. 3b main text).** (a) State residue: deviation of the system state from the target. (b) Control residue: the deviation of the control variable from its baseline value.

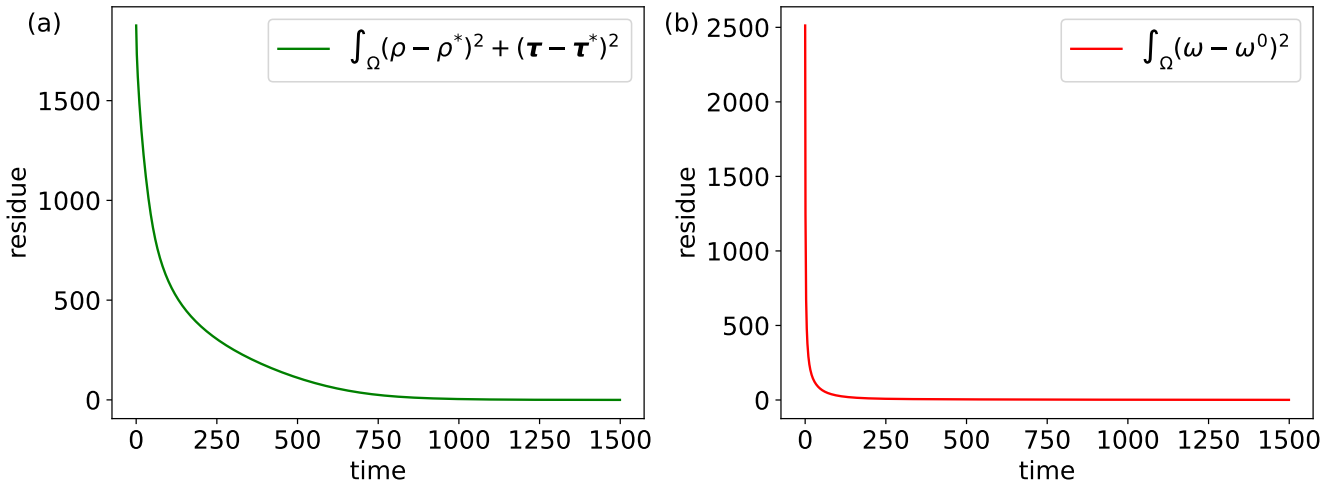

FIG. 4. **Residues for example in which a propagating stripe is remodelled into a stationary aster (Fig. 5 main text).** (a) State residue: deviation of the system state from the target. (b) Control residue: the deviation of the control variable from its baseline value.

VIII. MOVIE DESCRIPTIONS

- **Movie S1**: Aster translocation and reformation in the case where only the final state of the aster is specified (Fig. 2 main text). The left panel depicts density ρ (color map) and polarization $\boldsymbol{\tau}$ (arrows) profiles. The right panel shows the activity field ω, with a logarithmic scale colorbar.
- **Movie S2**: Aster translocation and reformation where the trajectory of aster is specified, with slow advection (Aster-like trajectory, Fig. 3a main text). The left panel depicts density ρ (color map) and polarization $\boldsymbol{\tau}$ (arrows) profiles. The right panel shows the activity field ω, with a logarithmic scale colorbar.
- **Movie S3**: Aster translocation and reformation where the trajectory of aster is specified, with fast advection (Flock-like trajectory, Fig. 3b main text).. The left panel depicts density ρ (color map) and polarization $\boldsymbol{\tau}$ (arrows) profiles. The right panel shows the activity field ω, with a logarithmic scale colorbar.
- **Movie S4**: Reorienting the direction of propagation of a stripe by 45^0 (Fig. 4 main text). The left panel depicts density ρ (color map) and polarization $\boldsymbol{\tau}$ (arrows) profiles. The right panel shows the activity field ω, with a logarithmic scale colorbar.
- **Movie S5**: Remodelling a propagating stripe to a stationary aster (Fig. 5 main text). The left panel depicts density ρ (color map) and polarization $\boldsymbol{\tau}$ (arrows) profiles. The right panel shows the activity field ω, with a logarithmic scale colorbar.
- **Movie S6**: Reorienting the direction of propagation of a stripe by 90^0. The left panel depicts density ρ (color map) and polarization $\boldsymbol{\tau}$ (arrows) profiles. The right panel shows the activity field ω, with a logarithmic scale colorbar.

[1] R. Kerswell, C. C. Pringle, and A. Willis, Reports on Progress in Physics **77**, 085901 (2014).
[2] A. Borzì and V. Schulz, *Computational optimization of systems governed by partial differential equations* (SIAM, 2011).
[3] D. E. Kirk, *Optimal control theory: an introduction* (Courier Corporation, 2004).
[4] S. Lenhart and J. T. Workman, *Optimal control applied to biological models* (Chapman and Hall/CRC, 2007).
[5] S. L. Brunton and J. N. Kutz, *Data-driven science and engineering: Machine learning, dynamical systems, and control* (Cambridge University Press, 2022).
[6] S. Skogestad and I. Postlethwaite, *Multivariable feedback control: analysis and design* (john Wiley & sons, 2005).
[7] K. J. Åström, *Introduction to stochastic control theory* (Courier Corporation, 2012).